J Physiol 599.8 (2021) pp 2239–2254

The Journal of Physiology

Loss of peripheral vestibular input alters the statistics of head movement experienced during natural self-motion

Omid A. Zobeiri[1], Benjamin Ostrander[2], Jessica Roat[2], Yuri Agrawal[2] and Kathleen E. Cullen[2,3,4,5]

[1]*Department of Biomedical Engineering, McGill University, Montreal, Quebec, Canada*
[2]*Department of Otolaryngology-Head and Neck Surgery, Johns Hopkins University, Baltimore, Maryland, USA*
[3]*Department of Biomedical Engineering, Johns Hopkins University, Baltimore, Maryland, USA*
[4]*Department of Neuroscience, Johns Hopkins University School of Medicine, Baltimore, USA*
[5]*Kavli Neuroscience Discovery Institute, Johns Hopkins University, Baltimore, USA*

Edited by: Richard Carson & Vaughan Macefield

Key points

- Sensory systems are adapted to the statistical structure of natural stimuli, thereby optimizing neural coding.
- Head motion during natural activities is first sensed and then processed by central vestibulo-motor pathways to influence subsequent behaviour, thereby establishing a feedback loop.
- To investigate the role of this vestibular feedback on the statistical structure of the head movements, we compared head movements in patients with unilateral vestibular loss and healthy controls.
- We show that the loss of vestibular feedback substantially alters the statistical structure of head motion for activities that require rapid online feedback control and predict this change by modelling the effects of increased movement variability.
- Our findings suggest that, following peripheral vestibular loss, changes in the reliability of the sensory input to central pathways impact the statistical structure of head motion during voluntary behaviours.

Abstract It is widely believed that sensory systems are adapted to optimize neural coding of their natural stimuli. Recent evidence suggests that this is the case for the vestibular system, which senses head movement and contributes to essential functions ranging from the most automatic reflexes to voluntary motor control. During everyday behaviours, head motion is sensed by the vestibular system. In turn, this sensory feedback influences subsequent behaviour, raising the questions of whether and how real-time feedback provided by the vestibular system alters the statistical structure of head movements. We predicted that a reduction in vestibular feedback would alter head movement statistics, particularly for tasks reliant on rapid vestibular feedback. To test this proposal, we recorded six-dimensional head motion in patients with variable degrees of unilateral vestibular loss during

Omid A. Zobeiri earned his BSc in electrical engineering and MSc in biomedical engineering at the Sharif University of Technology (Iran). He then travelled to Montreal, Canada, to start his PhD at McGIll University in Dr Kathleen Cullen's lab. During his PhD, he has been studying how vestibular signals are integrated with other sensory and motor information during voluntary behaviours in human and animal models.

DOI: 10.1113/JP281183

standard balance and gait tasks, as well as dynamic self-paced activities. While distributions of linear accelerations and rotational velocities were comparable for patients and age-matched healthy controls, comparison of power spectra revealed significant differences during more dynamic and challenging activities. Specifically, consistent with our prediction, head movement power spectra were significantly altered in patients during two tasks that required rapid online vestibular feedback: active repetitive jumping and walking on foam. Using computational methods, we analysed concurrently measured torso motion and identified increases in head–torso movement variability. Taken together, our results demonstrate that vestibular loss significantly alters head movement statistics and further suggest that increased variability and impaired feedback to internal models required for accurate motor control contribute to the observed changes.

(Received 2 December 2021; accepted after revision 16 February 2021; first published online 18 February 2021)
Corresponding author K. E. Cullen: Department of Biomedical Engineering, Johns Hopkins University, Baltimore, Maryland, USA. Email: kathleen.cullen@jhu.edu

Introduction

The vestibular system senses movements of the head in space. These head movements can occur due to either passive activities (e.g. riding in a car) and/or active, self-generated activities (e.g. walking, running). Recent studies have characterized the statistical structure (e.g. the probability of occurrence, and the spectral frequency content) of head movements occurring during natural activities in both humans and non-human primates (Carriot *et al.* 2014; 2017a; Hausamann *et al.* 2019). Importantly, in response to the head movements experienced during natural activities, the vestibular system influences subsequent behaviour via the generation of vestibular reflexes and/or the updating of internal models required for accurate motor control (reviewed in Clark *et al.* 2019; Cullen 2019). Accordingly, these motor behaviours generate head movements that, in turn, stimulate the vestibular system. The fact that this essential sensory system also makes important contributions to motor behaviour raises the fundamental question of whether and how such real-time feedback provided by the vestibular system alters the statistical structure of natural head movements. Time-domain analyses have revealed significant differences in the amplitude, velocity and variability of head movements during natural behaviours such as voluntary head movements and locomotion in patients with bilateral (Pozzo *et al.* 1991; Sağlam *et al.* 2014) and complete unilateral vestibular loss (Mijovic *et al.* 2014; Paul *et al.* 2017, 2018; Zobeiri *et al.* 2021). Yet, to date, how the loss of vestibular feedback affects the frequency content of head movements experienced during natural activities remains unknown.

In healthy individuals, the vestibular sensory organs on each side of the head detect head movement in six dimensions (three axes of translation and three axes of rotation) to ensure stable gaze and provide our sense of self-motion. However, following peripheral vestibular loss, individuals demonstrate deficits in gaze stability as well as impairments in balance and postural control (Mergner *et al.* 1991; Minor 1998; Macpherson and Fung 1999). These symptoms can be debilitating, making it difficult for patients to perform their normal everyday activities. Specific clinical measures that commonly reveal abnormalities in vestibular function include quantification of the vestibulo-ocular reflex, postural sway testing, and the 10-task functional gait assessment (FGA) (reviewed in Baloh *et al.* 2010; Hullar *et al.* 2010; Goldberg *et al.* 2012; Nnodim and Yung 2015). Notably, the increased postural sway and impairments revealed by FGA testing observed in patients with peripheral vestibular loss could impact the statistical structure of head motion in the frequency domain during these exercises, as well as during other voluntary behaviours relative to normal subjects.

Accordingly, here we investigated the role of vestibular feedback on the statistics of head movements during voluntary activities, in both the frequency and temporal domains. We hypothesized that the reduction in head motion feedback would alter the statistics of the vestibular signals experienced during active, self-generated motion in patients with variable degrees of unilateral vestibular loss when compared with healthy controls. In particular, we predicted differences in the statistical structure of head movement would be most marked during tasks most dependent on vestibular feedback, such as walking on foam (during which the reliability of other short-latency sensory feedback from the somatosensory system is reduced) and dynamic tasks that require rapid online feedback control. To test this proposal, we measured six-dimensional head motion during standard clinical assessments that included the 10-task FGA. Additionally, because head motion is likely restricted to a more limited range for these assessments than

that which is experienced during everyday activities, we also measured six-dimensional head movements during more challenging dynamic activities designed to better represent the full range of movements potentially encountered in daily life, including: (1) walking on foam, (2) jumping and hopping, (3) quickly locomoting around obstacles, and (4) a self-paced dish-sorting task. Consistent with our prediction, we found that vestibular loss substantially altered the statistical structure of head movements for activities requiring rapid and robust online vestibular feedback. Using computational methods, we next demonstrated that the observed changes in frequency content could be predicted by modelling the effect of head–torso coupling. Notably, in contrast to prior time-domain based analyses, our frequency-based approach identified head movement differences in a clinical population largely comprised of patients with only partial unilateral vestibular loss. Thus, taken together, our results suggest that the increased variability of vestibulospinal reflexes and the lack of accurate updating of internal models alter the head movement statistics experienced during activities requiring robust online feedback control.

Methods

Ethical approval

Written informed consent was obtained and all procedures were approved by the Johns Hopkins University Institutional Review Board (NA-00087648). The study was conducted in accordance with the *Declaration of Helsinki*, except for registration in a database.

Subjects

Two groups of participants were recruited for this study from the otolaryngology clinic. The first study group consisted of 10 patients (mean age 61.5 years, range 45–80 years, four females) with chronic unilateral vestibular hypofunction: seven patients diagnosed with chronic unilateral vestibular hypofunction due to various aetiologies (e.g. Meniere's disease, vestibular neuritis) and three patients with unilateral vestibular loss as a result of vestibular schwannoma resection. All patients had evidence of unilateral vestibular loss based on bithermal caloric irrigation testing (unilateral weakness >25%) and/or quantitative video–head impulse testing (vestibulo-ocular reflex gain <0.7 in the affected ear, normal in the unaffected ear), per published criteria (Strupp & Magnusson, 2015). The second group included 10 age-matched, sex-matched controls (mean age 60.5 years, range 45–79 years, four females) who did not have any history of otologic or neurologic disease.

Movement recordings

Each subject's head-in-space (H_S) and torso-in-space (T_S) movements were recorded in six dimensions using two micro-electromechanical systems (MEMS) wireless sensors (Shimmer3, Shimmer Research Ltd, Dublin, Ireland), each comprising three linear accelerometers (recording linear accelerations along the fore-aft, inter-aural, and vertical axes) and three gyroscopes (recording angular velocity about pitch, roll and yaw; Fig. 1*A*). Data from each sensor was sampled at 1000 Hz and recorded on a microSD card. Before each recording session, the Shimmer3 sensor accelerometers and gyroscopes were calibrated using the manufacturer's recommended approach (Ferraris *et al.* 1995). During experiments, one of these small (51 mm × 34 mm × 14 mm) light-weight (26 g) sensors was comfortably attached to the subject's head (above the left ear) to measure angular velocities and linear accelerations referenced as close to the vestibular end organs as possible (see Carriot *et al.* 2014, 2017a,b). The second sensor was placed on the torso (i.e. near L2–L3). For the head sensor, the plane spanned by the fore-aft and the lateral axis of the Shimmer3 was visually aligned with the subject's Frankfurt plane (i.e. the plane passing through the inferior margin of the orbit to the external auditory meatus). To further confirm the alignment to the Frankfurt plane, we recorded the acceleration while subjects were positioned stationary and confirmed that the *z*-axis of the sensor was aligned to gravity. In case of small errors, a corrective rotation matrix was estimated and applied to both 3-axis accelerometer and gyroscope.

Functional gait assessment (FGA)

Patients were tested using the standard FGA which is commonly used in the clinic to assess postural stability during walking and comprises 10 tasks (Wrisley *et al.* 2004). Specifically, we recorded six-dimensional head and torso movements during these standard tasks which include: (1) gait on a level surface, (2) change in gait speed, (3) gait with horizontal head turns, (4) gait with vertical head turns, (5) gait and pivot turn, (6) step over obstacle, (7) gait with narrow base of support, (8) gait with eyes closed, (9) ambulating backward, and (10) steps.

Additional dynamic activities

In addition to the testing done for FGA tests, we recorded six-dimensional head and torso movements during dynamic activities designed to emulate movements

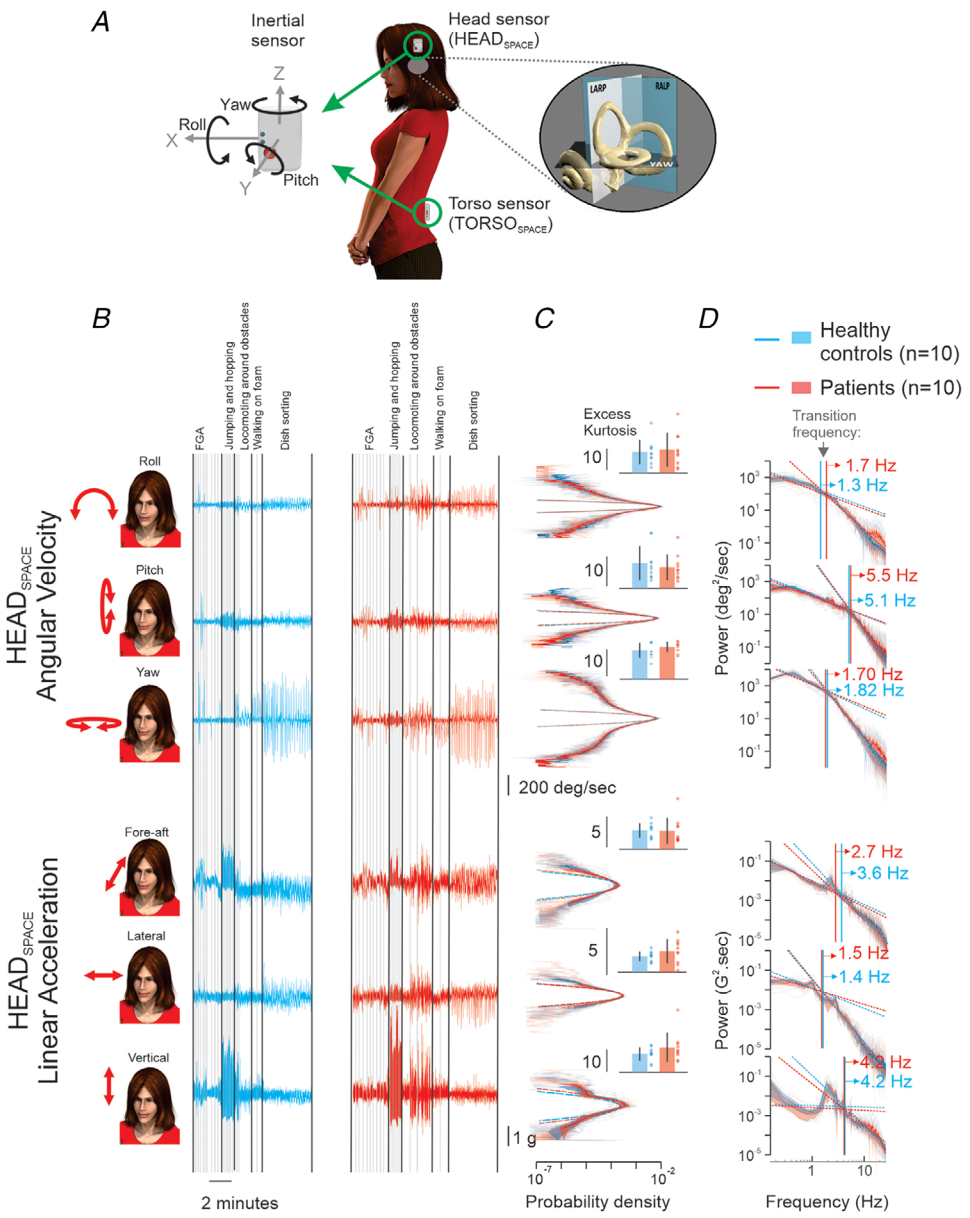

Figure 1. Distributions of head linear accelerations and rotational velocities were comparable for patients and healthy controls during all activities
A, head-in-space (H_S) and torso-in-space (T_S) movements in six dimensions were recorded using two lightweight inertial sensors. *B*, an example of H_S roll angular velocity (first row), pitch angular velocity (second row), yaw angular velocity (third row), fore-aft acceleration (fourth row), lateral linear acceleration (fifth row), and vertical linear acceleration (sixth row) signals during all tested tasks, recorded from one healthy control (blue traces) and one unilateral vestibular patient (red traces). *C*, the population-averaged probability distributions of vestibular stimuli (angular velocity or linear acceleration) in all six motion dimensions for healthy controls (blue) and unilateral vestibular patients (red). Insets: population-averaged excess kurtosis values (patients *vs*. healthy controls; roll: 14.1 ± 8 *vs*. 13 ± 5.79, $P = 0.74$; pitch:10.1 ± 4.37 *vs*. 11.5 ± 5.76, $P = 0.54$; yaw: 15.3 ± 1.99 *vs*. 14 ± 2.89, $P = 0.26$; fore-aft: 6 ± 2.14 *vs*. 6.07 ± 1.18, $P = 0.94$; lateral: 5.29 ± 1.3 *vs*. 4.73 ± 0.53, $P = 0.22$; vertical: 15 ± 6.92 *vs*. 11.9 ± 3.19, $P = 0.23$). *D*, population-averaged power spectra of these signals with corresponding 95% confidence intervals (shaded bands) superimposed on the power spectra of individual subjects. Dashed lines show the power-law fits over the low-frequency and the high-frequency ranges. The transition frequencies (i.e. the frequency at which the power-law fits intersect) are also shown for both healthy controls and patients. [Colour figure can be viewed at wileyonlinelibrary.com]

experienced in daily life, including: (1) jumping and hopping, (2) walking on foam, (3) locomoting around obstacles and (4) self-paced dish-sorting. During the 'jumping' and 'hopping' tasks, each subject first jumped 10 times as high as they could, then after a 15 s pause hopped on each foot 10 times (right then left). The 'jumping' and 'hopping' tasks were each repeated twice. During the 'walking on foam' tasks, subjects initially stood on a firm floor then stepped onto and walked ∼3 steps along an Airex foam balance-beam (160 × 24 cm, Airex AG, Sins, Switzerland). This task was performed with the subject either walking with both feet or a single foot on the foam, and each task was repeated twice. During the 'locomoting around obstacles' tasks, subjects were instructed to (i) walk, (ii) run, and finally (iii) dribble a soccer ball around three cones placed 5 feet apart. Subjects began 5 feet from the first cone and turned around the last cone to repeat the sequence in reverse, returning to the start point. Finally, during the 'dish-sorting' task subjects started facing a shelving unit (IKEA KALLAX, 77 × 147 cm) and were asked to pick up plastic plates, cups and utensils (IKEA, KALAS) one by one from a basket on a table (75 cm high) located on their left side. They were instructed to sort them as quickly as possible into six groups by colour to match examples of each colour that had been previously positioned on each of six shelves.

Data analysis

For each activity, we quantified the distribution of the motion signals measured by the two sensors (head and torso) for each of the six axes of motion (three linear and three rotational axes). Specifically, for each subject, sensor, and axis we first removed the mean of the signal and then computed the kurtosis and root mean square (RMS) for each activity defined as follows:

$$Kurtosis = \frac{\frac{1}{n}\sum_{i=1}^{n} x_i^4}{\left(\frac{1}{n}\sum_{i=1}^{n} x_i^2\right)^2} \quad (1)$$

$$RMS = \sqrt{\frac{1}{n}\sum_{i=1}^{n} x_i^2} \quad (2)$$

in which $x_i\,(i = 1\ to\ n)$ are data samples and n is the length of the signal. In addition, we performed a frequency-dependent analysis of these same movements. Specifically, we first computed the power spectral densities (Pwelch function, MATLAB, MathWorks) using Welch's averaged periodogram with nfft = 2048 and a Bartlett window (2048 ms duration, corresponds to 0.488 Hz frequency resolution) for all six dimensions of movement recorded by each of the two sensors. We fit the power spectrum with a power law over both the low- and high-frequency ranges by finding two lines that could best represent (i.e. highest R^2) the power spectrum between the range of 0.2 Hz to 30 Hz (Carriot *et al.* 2014). These ranges correspond to those used in neurophysiological studies (Massot *et al.* 2012). In the fore-aft and vertical axes, which comprised significant power at the locomotion frequency (∼2 Hz), we excluded the power at the frequencies from 1 Hz to 3 Hz in our fitting algorithm. The transition frequency was determined as the frequency at which the two power-law fits intersected. To find the difference between the power spectra of two groups, we determined every frequency band larger than 5 Hz in which the power was significantly different at all frequencies within the band.

We also computed head-on-torso motion (H_T) spectra by taking the spectra of the difference between the corresponding (i.e. same sensor and axes) H_s and T_s signals. Additionally, we adapted the approach of Miyamoto *et al.* 2020, in which signals from the head (H_s) and torso (T_s) sensors were first filtered (5th order Butterworth zero-phase bandpass filters, with cut-off frequencies of 0–5, 5–10, 10–15, 15–20 and 20–25 Hz). For each frequency band, the zero-crossings of the resultant signals were used to identify the beginning and end of band-specific cycles. To obtain gain estimates G_{HT} and G_{HS}, H_T and H_S signals were divided by corresponding T_S signals, respectively. Similarly, $Phase_{HT}$ was defined as the phase difference between H_T and T_S signals in degrees. For our 5 Hz-wide bandpass-filtered motion signals, we computed the gain and phase values using a linear regression analysis performed on each individual cycle. For each frequency band, the manifold that explains G_{HS} as a function of G_{HT} and $Phase_{HT}$ was estimated by fitting a surface on the values across all cycles from all subjects.

Statistics

To confirm that the power of the spectrum remained significant at a given frequency, we recorded the motion signals for 15 min while the motion sensor was not moving to determine the motion sensor's noise level. We then computed and compared the power spectral density of the noise with that of the recording signals during different activities. For all comparisons between measures from healthy controls and vestibular patients, we performed independent sample permutation tests. Specifically, *P*-values were computed, obtaining the test statistics for 10,000 randomized rearrangements of the observed data points. These measures include RMS, kurtosis, power at each frequency point and any specific frequency band, as well as the variability and deviation of the average of G_{HT} and $Phase_{HT}$. All significant effects are reported at $P < 0.05$. Correction for multiple comparisons

was not performed since the goal of this exploratory study of was to investigate unilateral vestibular loss patients already known to be different from healthy controls based on clinical assessment and performing correction would have exaggerated Type II errors. Throughout the text, values are expressed as means ± SD. All data processing and statistical tests were performed using MATLAB (The MathWorks, Inc., Natick, Massachusetts, United States).

Results

Statistics of natural self-motion signals in patients with vestibular loss

We examined motion along six axes (three translational and three rotational motion) in 10 individuals with vestibular loss and 10 controls during the 10-task FGA as well as more challenging dynamic activities designed to better represent the full range of movements potentially encountered in daily life. These included walking on foam, jumping and hopping, locomoting around obstacles and dish-sorting. The time-varying profiles and distribution of the head motion signals recorded from one healthy control (blue traces) and one unilateral vestibular patient (red traces) in each of the three axes of translation and three axes of rotation are shown in Fig. 1*B* and 1*C*, respectively. Notably, the intensity of these stimuli reached up to 500°/s of angular velocity and 2 *g* of linear acceleration (Fig. 1*B*).

We found that the overall intensity of vestibular stimuli did not differ between patients and control participants. Specifically, to determine whether the range of head-in-space (H_S) movement values differed for patients *versus* controls for the three rotational and three linear axes, we first computed the RMS of the motion experienced across all tasks in our study. We found no difference in RMS for any of the six dimensions of head motion ($P > 0.05$ for all axes). We also found that for both groups, the probability distributions across all activities for each of the six motion dimensions were not Gaussian, as quantified by large (>10) positive excess kurtosis values (Fig. 1*C*, insets), but were instead characterized by long tails implying that stimuli with high intensities were more likely to occur. Overall, the population-averaged excess kurtosis values were significantly different from zero for both groups, for all axes (highest $P = 0.0215$). Notably, we found no differences between the excess kurtosis values characterizing the distributions of experienced motion by healthy controls and unilateral vestibular patients (Table 1, $P > 0.05$ for all axes), with all values as those previously reported in our study of normal subjects (Carriot *et al.* 2014).

We next quantified the frequency content of vestibular stimuli by computing the power spectra of H_S motion across all activities. We found that for both healthy controls and unilateral vestibular patients, the power spectra generally decreased slowly for frequencies below ∼1–5 Hz and more sharply for higher frequencies (Fig. 1*D*). As a result, the spectra of natural self-motion signals were not well fit by a power law (Fig. 1*D*), again consistent with previous findings in normal human subjects (Carriot *et al.* 2014). Specifically, the best power-law fit obtained over the low-frequency range gave rise to a different exponent (which corresponds to the slope of the fit on a log-log plot) than the best power-law fit obtained over the high-frequency range (see Methods). This 'transition frequency' is denoted for each spectrum in Fig. 1*D* (vertical lines).

Vestibular stimuli statistics in patients are altered for challenging and dynamic tasks

Our analysis above considered the vestibular stimuli experienced across all activities. This raises the question of whether there are differences in the statistical structure of the vestibular stimuli experienced by patients and control subjects for specific behaviours. To answer this question, we next compared the H_S motion of our patients and control subjects in all dimensions within each task. Interestingly, we again found no significant differences between the RMS and/or kurtosis values between our two subject groups for each of our specific tasks in any dimension. We then compared the power spectra of the vestibular stimuli generated by subjects during each of these activities. Fig. 2 illustrates all the frequency bands (See Methods) across which the power spectral density of H_S movements experienced by unilateral vestibular patients *versus* healthy controls were significantly different. Rows represent different activities, while columns correspond to the motion measured in each of the six axes. Red-filled areas represent frequency ranges over which patients showed significantly higher power than healthy controls.

Overall, we found that: (i) Patients experienced a significant increase in high-frequency power in vertical H_S acceleration during both trials of vertical jumping (Fig. 2, open orange rectangles). (ii) Patients also experienced greater high-frequency H_S roll power during two challenging activities in which subjects walked on a narrow foam 'balance-beam' (see Methods) with either both feet or a single foot (Fig. 2, open green rectangles, top and bottom, respectively). (iii) Finally, patients experienced decreased power in all linear motion axes during a standard FGA task requiring changes in gait speed (Fig. 2, open purple rectangles). Notably, we were surprised to find no difference in the head movement power experienced by patients *versus* controls during the 'dish-sorting' task, a task that required subjects to rapidly generate directed head and body movements. Both subject groups also completed the task in a comparable period of

Table 1. Kurtosis of head motion (mean ± SD)

Task group	Axis of motion	Patients	Healthy controls	*P*
Functional gait assessment	Roll	26.7 ± 16.7	24.2 ± 11.4	0.71
	Pitch	17 ± 5.73	23.6 ± 10.5	0.10
	Yaw	14.9 ± 7	18.7 ± 9.07	0.30
	Fore-aft	7.23 ± 2.53	7.84 ± 1.99	0.55
	Lateral	3.68 ± 0.70	3.93 ± 1.74	0.78
	Vertical	6.34 ± 1.15	7.15 ± 2.89	0.44
Jumping and hopping	Roll	7.3 ± 3.67	5.05 ± 2.09	0.11
	Pitch	4.05 ± 1.49	4.76 ± 1.8	0.36
	Yaw	5.58 ± 1.74	4.43 ± 1.38	0.11
	Fore-aft	4.26 ± 1.7	3.95 ± 1.07	0.63
	Lateral	4.68 ± 1.83	3.73 ± 0.611	0.14
	Vertical	2.58 ± 0.9	2.58 ± 0.852	0.99
Locomoting around cones	Roll	5.93 ± 2.25	5.41 ± 1.08	0.54
	Pitch	5.11 ± 1.16	5.8 ± 2.25	0.4
	Yaw	5.06 ± 2.37	4.96 ± 1.59	0.91
	Fore-aft	4.6 ± 0.83	4.7 ± 1.18	0.83
	Lateral	3.83 ± 1.17	3.82 ± 0.68	0.97
	Vertical	7.49 ± 3.02	6.62 ± 2.2	0.47
Walking on foam	Roll	5.61 ± 1.81	4.31 ± 1.01	0.064
	Pitch	5.53 ± 2.54	5 ± 3.93	0.76
	Yaw	6 ± 0.797	5.94 ± 1.91	0.94
	Fore-aft	4.7 ± 1.35	4.41 ± 1.3	0.62
	Lateral	3.94 ± 2.2	2.86 ± 0.38	0.11
	Vertical	9.12 ± 6.25	6.5 ± 2.04	0.22
Dish sorting	Roll	6.92 ± 1.85	6.86 ± 2.78	0.96
	Pitch	5.94 ± 1.57	5.28 ± 1.16	0.31
	Yaw	8.22 ± 3.47	6.92 ± 1.38	0.31
	Fore-aft	2.93 ± 0.52	2.93 ± 0.44	0.98
	Lateral	4.46 ± 1.08	3.91 ± 0.98	0.25
	Vertical	4.88 ± 2.22	4.17 ± 1.31	0.39

time ($P = 0.64$). However, we did find that patients made significantly more head turns in the direction ipsilateral to the lesion than controls, consistent with a prior report (Mijovic *et al*. 2014).

To demonstrate the increase in H_S motion power during the 'jumping' (Fig. 3*A*) and 'walking on foam' tasks (Fig. 3*C*) observed in patients (i.e. Fig. 2, open orange and green rectangles, respectively), we superimposed their population-averaged power spectra on those of control subjects. Overall, during the 'vertical jumping' task, patients experienced greater linear vertical H_S motion power at higher frequencies (Fig. 2, open orange rectangles, Fig. 3*B*, shaded grey area; 10–18 Hz, $P = 0.0086$). Importantly, since we collected data for two trials of the 'jumping' task, we were further able to validate that this result was consistent across both the first and second set of trials (Fig. 2, open orange rectangles). Likewise, during the 'walking on foam' task, patients again experienced greater H_S motion power at higher frequencies. Specifically, comparison of patient and control subject data during the 'walking on foam with both feet' task revealed that patients generated significantly higher power in their side-to-side H_S rotations (i.e. roll axis) (Fig. 2, top open green rectangle, Fig. 3*D*, shaded grey area; 10–25 Hz, $P = 0.047$). Further, during the 'walking on foam with one foot' task, patients also generated significantly higher power in the roll axis (Fig. 2, bottom green rectangle, 1225 Hz, $P = 0.043$). Notably, the results of our frequency-based analysis of these tasks were in striking contrast to those obtained by quantifying the temporal-based RMS or probability distribution motion amplitude in each dimension, as noted above. Specifically, comparison of RMS between control and patient groups revealed no differences for vertical accelerations or any of the other remaining five dimensions of H_S motion (Figs. 3*A* & *C*, *bottom insets*; $P = 0.67$ and $P = 0.79$, for jumping and walking on foam with one foot or both feet, respectively). A comparison of kurtosis values likewise revealed no differences between groups ($P = 0.32$ and $P = 0.62$).

Finally, as shown in Fig. 2 (open purple rectangles), we only observed a difference in H_S motion power for patients *versus* controls during one of the more challenging gait tasks within the standard FGA. Specifically, during the task requiring 'changes in gait speed' (Fig. 4*A*), patients experienced a relative decrease in power for motion along all linear axes at higher frequencies (Fig. 4*B*, denoted by shaded grey areas; fore-aft 18–25 Hz, $P = 0.043$; lateral, 15–22 Hz, $P = 0.025$; vertical, 18–25 Hz $P = 0.026$). Fig. 4*B* directly compares the population-averaged power spectrum of patients and control subjects for the 'change in gait speed' task of FGA (Fig. 2, open purple rectangles). Again, the results of our frequency-based analysis of these tasks contrasted with those obtained by quantifying the RMS or probability distributions of movement in each dimension. Notably, the RMS of head motion experienced by vestibular patients and healthy controls was again comparable during the 'change in gait speed' task (Fig. 4*A* bottom inset; $P = 0.55$, $P = 0.85$, $P = 0.22$), and comparison of kurtosis revealed no differences between the distributions of motion in any direction between the two subject groups ($P = 0.36$, $P = 0.56$ and $P = 0.67$).

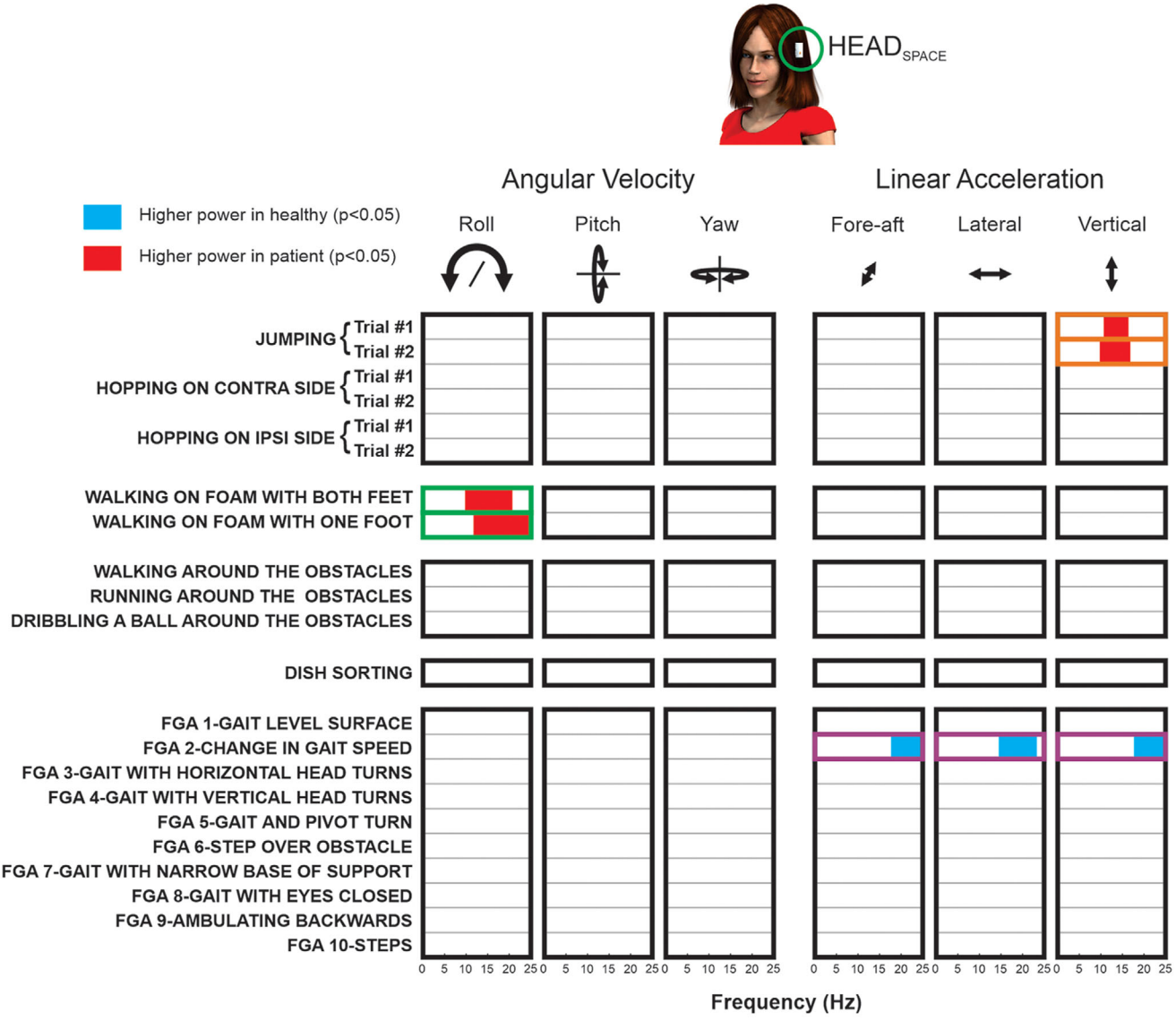

Figure 2. Overview of the differences in the power spectra of H_S movements for all six motion dimensions (columns) experienced by unilateral vestibular patients *versus* healthy controls, during all tested tasks (rows)
Red- and blue-filled areas represent frequency ranges over which patients showed significantly higher power than healthy controls, respectively ($P < 0.05$). Green and orange open rectangles highlight the tasks and axes of motion in which patients experienced different head movements from healthy controls. [Colour figure can be viewed at wileyonlinelibrary.com]

Power spectra analyses further reveal differences in torso motion / head-on-torso motion for vestibular patients during jumping

In addition to recording six-dimensional head motion relative to space, we simultaneously recorded six-dimensional torso motion relative to space (T_S) during all activities. As observed in our analysis of head motion, the RMS and kurtosis of torso motion experienced by vestibular patients and healthy controls was likewise comparable in all tasks for all six axes ($P > 0.057$, for both measures). Interestingly, comparison of T_S motion power in each axis revealed no differences between patients *versus* healthy control subjects for the majority of tasks. However, we did observe differences during three specific tasks. First, patients experienced decreased high-frequency T_S power in the fore-aft axis during two tasks of the FGA namely, (i) gait with horizontal head turns (20–25 Hz; $P = 0.014$) and (ii) gait and horizontal body pivot turns (20–25 Hz; $P = 0.012$). However, patients did not demonstrate corresponding differences in head motion during these same tasks (Fig. 2). Importantly, patients also experienced a relative increase in linear vertical torso movement power compared with healthy controls during the 'vertical jumping' task (Fig. 5*A*, left panel, denoted by shaded grey area). Indeed, this change was similar to that described above for our analysis of head motion power during jumping, with patients generating higher power in their linear vertical torso movement relative to healthy controls at higher frequencies (14–22 Hz, $P = 0.032$).

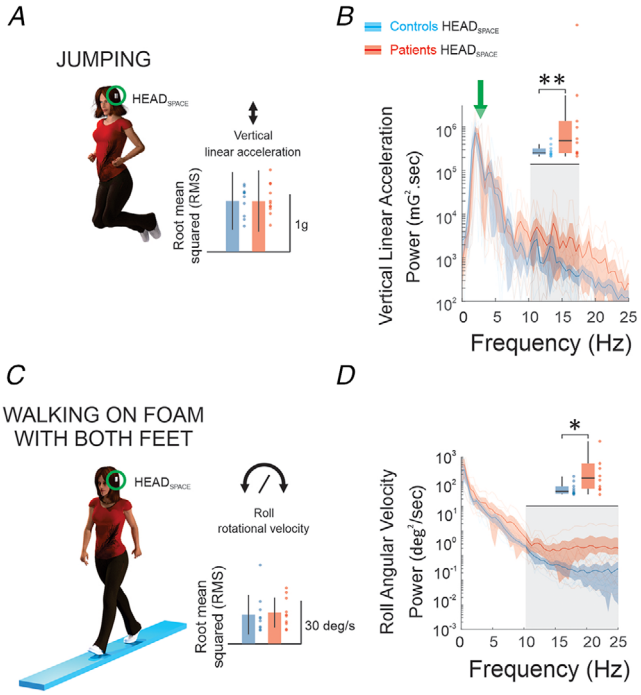

Figure 3. Patients experienced increased H_S motion power relative to control subjects during the 'jumping' and 'walking on foam' tasks
A, illustration of the 'jumping' task. Inset: Comparison of the root mean square (mean ± SD) of the H_S linear acceleration in vertical dimension during 'jumping' task. *B*, population-averaged power spectra with corresponding 95% confidence intervals (shaded bands) for healthy controls (blue) and patients (red) for the H_S vertical acceleration superimposed on the power spectra of individual subjects. Bar plot demonstrates median and quartile values of the normalized power over the frequency band denoted by the grey shaded area in the power spectra. *C*, illustration of the 'walking on foam with both feet' task. Inset: Comparison of the root mean square (mean ± SD) of the H_S rotational velocity in roll dimension during 'walking on foam with both feet' task. *D*, population-averaged power spectra of the H_S rotational velocity in roll dimension with corresponding 95% confidence intervals (shaded bands) for the 'walking on foam with both feet' superimposed on the power spectra of individual subjects. Bar plots demonstrate the median and quartile values of the normalized power over the frequency band denoted by the grey shaded area in the power spectra. (**: $P < 0.01$, ***: $P < 0.001$). [Colour figure can be viewed at wileyonlinelibrary.com]

To gain insight into the mechanisms underlying the observed increases in both head and torso power generated by patients during jumping, we next calculated the difference between concurrently measured head and torso motion to compute head motion relative to torso motion (H_T). Figure 5*A* (right panel) plots the power spectra for vertical linear H_T. Overall, H_T power was comparable for patients and healthy controls at lower frequencies of movement, consistent with relative similarity between torso and head motion power relative to space (H_S) for both groups (Fig. 5*A*, centre panel). Correspondingly, patients generated increased H_T power in the vertical axis at higher frequencies, consistent with an increased head–torso stabilization required for the higher T_S power generated in this range (Fig. 5*A*, right panel, shaded grey area, 10–20 Hz, $P = 0.049$).

Finally, as noted above, the torso motion generated by unilateral vestibular patients and healthy controls was comparable for the large majority of activities, across all six axes. Interestingly, this remained the case for the 'walking on foam' tasks described above (Fig. 3*C* & *D*), during which patients experienced significantly greater head movement (H_S) power in the roll axis at higher frequencies compared with healthy controls (Fig. 5*B*, left panel). Thus, the increase in roll head motion observed in this task was not related to a change in T_S. Thus, to gain insight into this result we again calculated the difference between concurrently measured head and torso motion to compute head motion relative to torso motion (H_T). Figure 5*B* (right panel) plots the power spectra for roll axis H_T. Surprisingly, we found that patients and controls experienced similar head motion relative to torso (H_T) across all frequencies (Fig. 5*B*, right, $P > 0.064$). This then raises the question: If head–torso coupling is comparable in patients and controls during walking on foam, how

can we interpret the observed difference in the H_S power spectra?

Head-on-torso variability increases for patients during challenging balance tasks

To further investigate this apparent paradox, we analysed the motion of each subject within specific frequency bands to assess the phase as well as within-subject variability of the head–torso coupling during the 'walking on foam' task. Specifically, adapting a method from Miyamoto *et al.* 2020, we first bandpass filtered the measured roll signals to obtain five equally spaced bands across the physiologically relevant frequency range (e.g. 0–5 Hz, …, 20–25 Hz) and then computed the average and variability of gain (G_{HT}) and phase ($Phase_{HT}$) of head–torso coupling for each frequency band-specific cycle (see Methods). Figure 6*A* plots the signals computed with the 20–25 Hz bandpass filter. Note that because our results revealed similar T_S motion in patients and healthy controls (Fig. 6*B*, left), increased H_S power at higher frequencies in vestibular patients is proportional to increased average of normalized frequency-dependent magnitude of H_S (i.e. G_{HS}). In theory, the G_{HS} is directly impacted by the average and variability of G_{HT} and $Phase_{HT}$. For instance, a sinusoidal movement can be described by G_{HT} and $Phase_{HT}$ based on a manifold that is shown in Fig. 6*B*. In this figure, joint distributions of G_{HT} and $Phase_{HT}$ are represented with the centre position (average) and radius (standard deviation) of the ovals. A perfect compensation (i.e. zero G_{HS}) only occurs when for all cycles the magnitude of H_T motion is equal to the T_S movement but in the opposite direction (i.e. centre position at $G_{HT} = 1$, $Phase_{HT} = 180°$ with zero radius, Fig. 6*B*, black stars). Any increase in the average distance of either G_{HT} or $Phase_{HT}$ values from this optimum point (i.e. change in centre or increase in radius of the oval) increase the G_{HS}. Thus, we hypothesized that the observed increase G_{HS} in the vestibular patients at high frequencies is due to an increased average distance of G_{HT} and $Phase_{HT}$ distributions from the optimal point.

Overall, four specific changes relative to a reference distribution (Fig. 6*B*, grey oval) could contribute to an increase in G_{HS}, specifically: (H1) a deviation in the average of G_{HT} from $G_{HT} = 1$ (Fig. 6*B*, open purple oval), (H2) a deviation of the average of $Phase_{HT}$ from

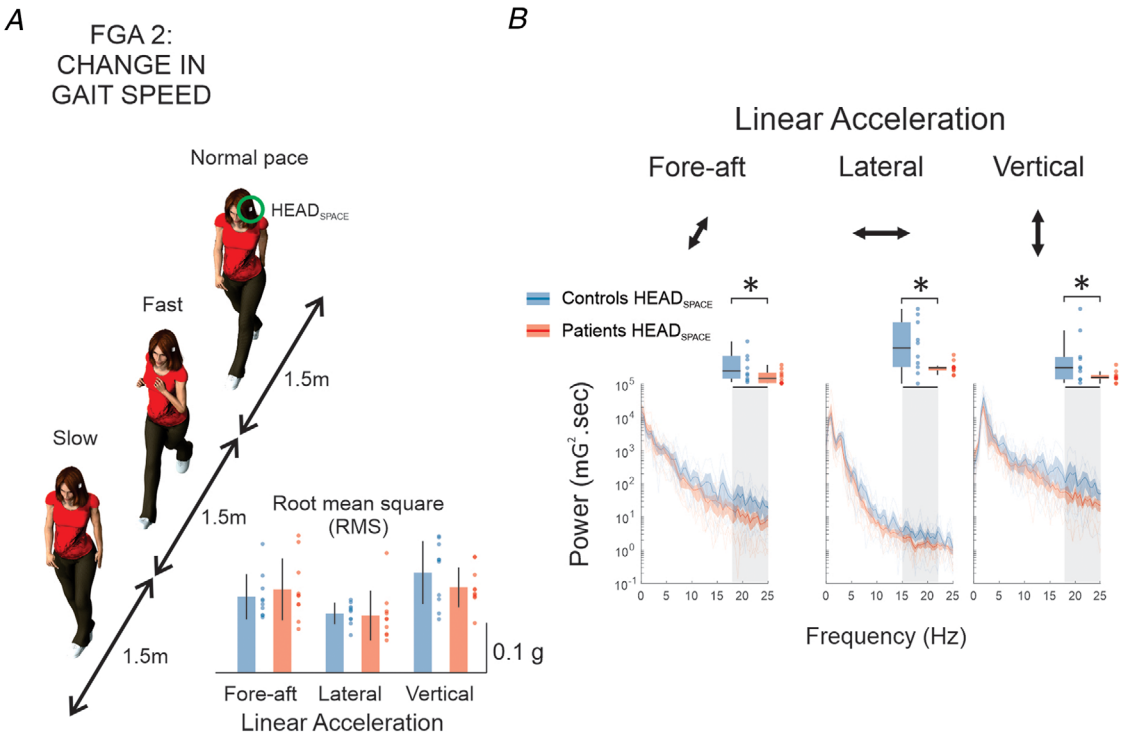

Figure 4. Patients experienced decreased H_S motion power during the 'change in gait speed' task of the FGA
A, illustration of 'change in gait speed' task. Inset: Comparison of the root mean square (mean ± SD) of the H_S acceleration in all three acceleration dimensions during 'change in gait speed' task. *B*, population-averaged power spectra with corresponding 95% confidence intervals (shaded bands) for healthy controls (blue) and patients (red) for three head acceleration axes. Bar plots demonstrate median and quartile values of the normalized power over the frequency bands denoted by the grey shaded area in the power spectra. (∗: $P < 0.05$) [Colour figure can be viewed at wileyonlinelibrary.com]

Phase$_{HT}$ = 180° (Fig. 6*B*, open green oval), (H3) an increase in the variability of G_{HT} (Fig. 6*B*, larger vertical radius of open orange oval), and (H4) an increase in the variability of the Phase$_{HT}$ (Fig. 6*B*, larger horizontal radius of open blue oval). Figure 6*C* plots the top view of the manifolds fitted on the data from our 'walking on foam' task. The blue and red ovals represent the joint distributions of G_{HT} and Phase$_{HT}$ for healthy controls and vestibular patients, respectively. Based on our results we ruled out our first possible hypothesis (H1), since the average G_{HT} in patients and controls were comparable across all frequency bands as illustrated by similar vertical position of the blue and red cross signs in Fig. 6*C* (Fig. 6*C*, top, H1, $P > 0.29$). This finding is further consistent with our power spectra analysis above showing that the H_T and T_S power spectra in patients and healthy controls were comparable (Fig. 5*B*). Second, our results also ruled out our second hypothesis (H2), since the average of Phase$_{HT}$ was comparable for patients and healthy controls (Fig. 6*C*, bottom, similar horizontal position of the blue and red cross signs, top: H2, $P > 0.25$). Notably, our data were consistent with our last two hypotheses (i.e. H3 and H4). Specifically, G_{HT} was significantly larger for vestibular patients than healthy controls at higher frequencies as illustrated by larger vertical radius of the red compared with the blue oval (Fig. 6C, top, H3, $P = 0.015$ for 10–15 Hz and $P = 0.013$ for 20–25 Hz). Also, the variability of Phase$_{HT}$ was significantly larger for vestibular patients than healthy controls at higher frequencies (Fig. 6C, top, H4, bottom: increased horizontal radius of red compared with blue oval; $P = 0.021$ for 15–20 Hz and $P = 0.019$ for 20–25 Hz). This result addresses the apparent paradox noted above, since it explains why patients have higher H_s power compared with controls during walking on foam even though both the power of T_s and head–torso coupling (H_T) were comparable. Specifically, patients generated higher variability in their head–torso coupling, which resulted in higher H_s power (Fig. 5*B*, middle).

Finally, for completeness, we performed a similar analysis on other activities in our dataset. First, we investigated the 'jumping' task, during which patients showed increased power in T_S, H_S and H_T compared with healthy controls between 10 and 20 Hz (i.e. Fig. 5*A*). Interestingly, our results again ruled out H1 and H2. Instead, again consistent with H3, we found that patients had significantly higher variability of G_{HT} compared with healthy controls at 10–15 Hz (Fig. 6*D*, $P = 0.023$), corresponding to the same region over which we saw increased power in patients. Further, although there was a tendency for increased Phase$_{HT}$ variability (i.e. H4) in patients, this did not reach significance. Thus, taken together, these findings suggest that patients commonly generated higher variability in their head–torso gain (i.e. G_{HT}) for these activities, consistent with H3.

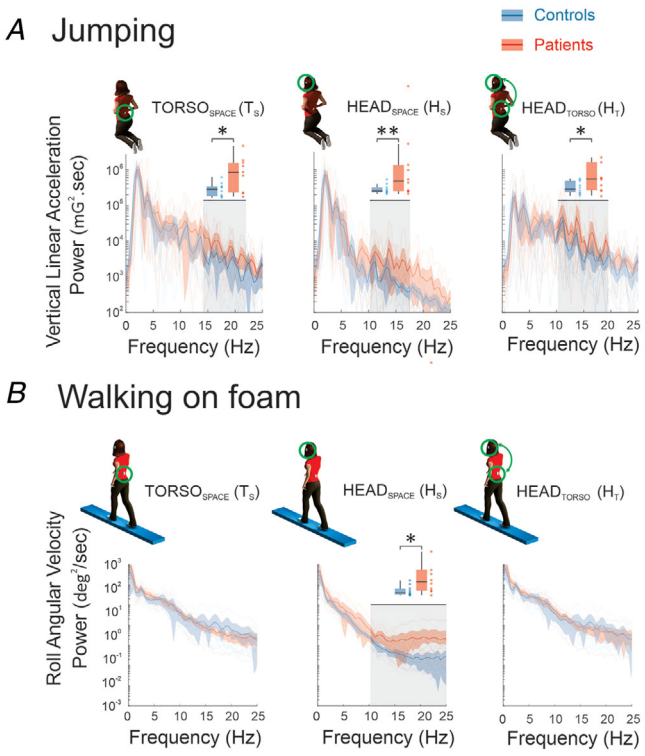

Figure 5. Patients experienced an increase in torso-in-space (T_S) and head-on-torso (H_T) power relative to control subjects during the 'jumping' task, but movement power spectra were comparable for both subject groups during the 'walking on foam' task
A, population-averaged power spectra for healthy controls (blue) and patients (red) for the T_S (left), H_S (middle), and H_T (right) vertical acceleration during the 'jumping' task superimposed on the power spectra of individual subjects. Bar plots demonstrate the median and quartile values of the normalized power averaged over the frequency bands denoted by grey shaded areas in the power spectra. *B*, population-averaged power spectra of the T_S (left), H_S (middle) and H_T (right) roll angular velocity with corresponding 95% confidence intervals (shaded bands) during the 'walking on foam' task superimposed on the power spectra of individual subjects. Bar plots demonstrate the median and quartile values of the normalized power over the frequency band denoted by grey shaded areas in the power spectra (**: $P < 0.01$). [Colour figure can be viewed at wileyonlinelibrary.com]

Discussion

Naturally occurring sensory stimuli are typically complex, and analyses that characterize these stimuli in both the time-based (temporal) and frequency domain are used to capture the complexity of the signals. For example, sounds can be described in either temporal (e.g. length of the sound, stimulus amplitude profile) or frequency (i.e. which frequencies of sound are present in the signal) domains. In the present study, we quantified the vestibular stimulation resulting from active movements in the temporal and frequency domains, to evaluate if and how the statistics of vestibular signals

during everyday activities are altered in individuals with vestibular loss. Specifically, we evaluated vestibular stimuli in the temporal domain by comparing the RMS and probability distributions of linear head accelerations and angular head velocities, and in the frequency domain by comparing the power spectral and frequency-dependent variability analyses of these same signals. We show for the first time that the spectral power of the vestibular signals experienced by patients differed from those experienced by control subjects. In particular, our data demonstrate that the loss of vestibular feedback alters the statistical structure of head movements experienced during most challenging activities that require robust online feedback control (i.e. jumping and walking on foam). To probe the underlying mechanisms, we analysed head and concurrently measured torso motion during each of our tasks and modelled the effect of head–torso coupling on the head stability. Based on these analyses, we suggest that increased variability in the head–torso coupling and compromised updating of the internal

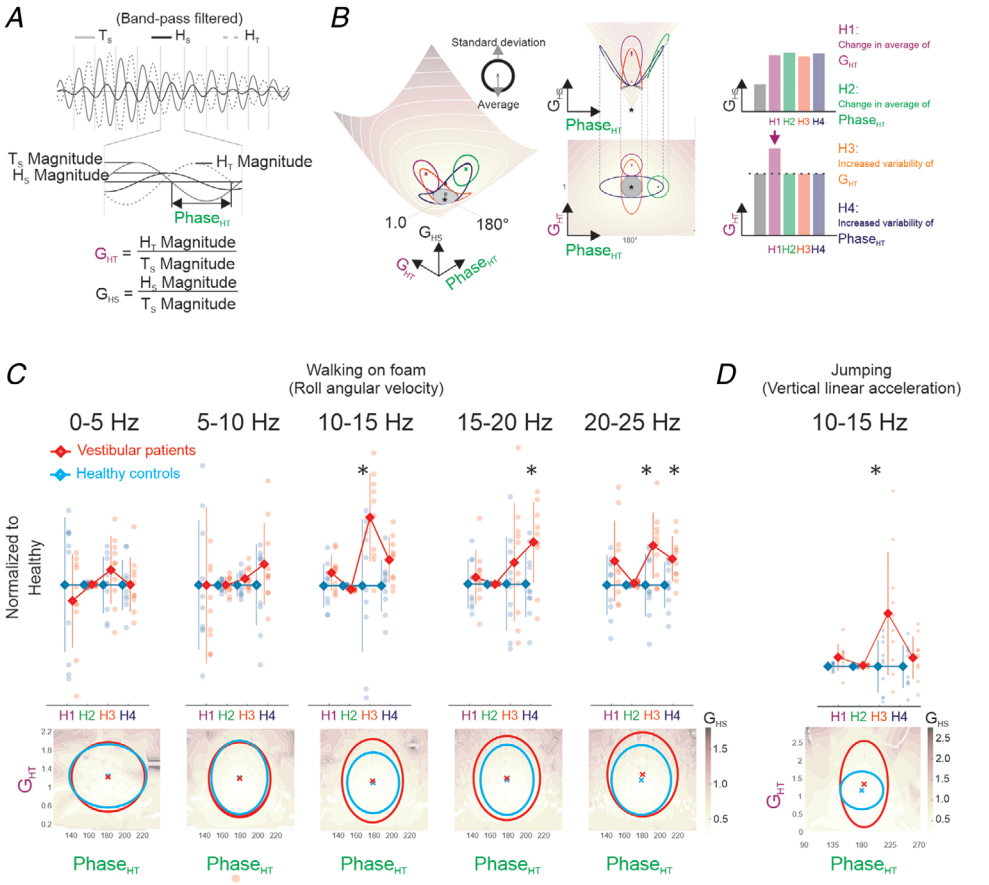

Figure 6. Vestibular patients generated more variable compensatory H_T motion during the 'walking on foam' and 'jumping' tasks
A, Top: an example of T_S (grey sold), H_S (black solid) and H_T (grey dashed) bandpass filtered at 20–25 Hz; *Bottom*: example of a single cycle of bandpass-filtered motion signal. *B*, Left: the theoretical manifold that explains the relationship between G_{HS}, G_{HT} and $Phase_{HT}$. The black star represents the perfect G_{HS} cancellation corresponding to $G_{HT} = 1$ and $Phase_{HT} = 180°$. The centre position (cross signs) and radius of the ovals represent the average and the standard deviation of five hypothetical distributions on the manifold. Four distributions that result in increased G_{HS} are compared with a hypothetical reference distribution (grey): H1 (purple) a change (increase or decrease) in the average of G_{HT}, H2 (green) a change in the average of $Phase_{HT}$, H3 (orange) an increase in the variability of G_{HT}, and H4 (dark blue) an increase in the variability of the $Phase_{HT}$. *C, Top*: a comparison of the four hypotheses from *B* for the roll angular velocity from the patients (red) and healthy controls (blue) for five different frequency bands during the 'walking on foam' task (mean ± SD). Increased head velocity in patients is consistent with the third hypothesis (H3) in the 10–15 and 20–25 Hz frequency bands and fourth hypothesis (H4) for 15–25 Hz. *Bottom*: illustration of the joint distribution of G_{HT} and $Phase_{HT}$ of patients (red) and healthy controls (blue) in different frequency bands. *D*, comparison of four different hypotheses for the vertical linear acceleration during the 'jumping' task in the 10–15 Hz frequency band. The results are consistent with the third hypothesis (H3) that shows significantly higher variability in G_{HT} in vestibular patients compared with healthy controls (∗: $P < 0.05$). [Colour figure can be viewed at wileyonlinelibrary.com]

models for challenging tasks requiring rapid online feedback contribute to the changes in the statistical structure of head motion observed following vestibular loss.

Vestibular loss alters head motion statistics of activities requiring online feedback

Our time-based analysis of vestibular stimuli first showed that patients with unilateral vestibular loss experience head movement intensities as high as 500°/s and 5.5 *g*. Amplitude distributions were comparable during each activity and across all six motion dimensions for patients and healthy controls. Specifically, distributions of both linear accelerations and rotational velocities were characterized by comparable large and positive excess kurtosis values in both groups. Additionally, head movement variability quantified using RMS was comparable. It is noteworthy that the majority of our subjects did not have a complete unilateral vestibular loss, as prior time domain-based analyses of head motion in the time domain have found differences between the head movements in populations of patients with complete unilateral vestibular loss (i.e. as a result of vestibular schwannoma surgery) and healthy controls (Mijovic *et al*. 2014; Paul *et al*. 2017, 2018; Zobeiri *et al*. 2021). In this context, our present findings are encouraging in that they provide evidence that while time-based measures lacked the sensitivity required to identify this specific group of patients, frequency-based analysis revealed marked differences between patients and healthy controls. For consistency, head motion signals are always measured with the sensor on the left side, rather than on the ipsilesional *versus* contralesional side. Nonetheless, we found that the probability distributions of the head motion for unilateral vestibular patients (Fig. 1*C*) were symmetrical, and not significantly different from controls, and thus we would not expect to see any significant differences in measurements made from sensors on the ipsilesional *versus* contralesional sides of the head.

In particular, our frequency-based analyses revealed that the vestibular signals experienced by patients with unilateral vestibular loss were altered for specific activities. Most notably, patients experienced significantly *greater* mid-to-high frequency head motion power while walking on foam and during jumping. Patients also experienced *lower* head motion power at higher frequencies in all three linear motion axes (fore-aft, lateral and vertical) during a standard FGA task requiring changes in gait speed. Taken together, our present results show that peripheral vestibular loss alters the statistical structure of the self-motion stimuli experienced during specific dynamic activities. Specifically, our findings suggest that patients with unilateral vestibular loss constrain their head movement during less challenging activities (e.g. gait on level surface and gait with head turns) but are unable to stabilize their heads during more challenging and/or dynamic activities (e.g. walking on foam and jumping).

Natural vestibular stimuli have significant frequency content up to ∼25 Hz in both humans and primates during active head turns (Armand & Minor, 2001; Huterer & Cullen, 2002), as well as during typical everyday activities including locomotion (Carriot *et al*. 2014, 2017a, b). When plotted in coordinates of log power *versus* log frequency, the power spectrum of such natural vestibular stimuli cannot be fit with a straight line (Carriot *et al*. 2014, 2017a). This contrasts with natural visual and auditory stimuli, which follow a relationship referred to as a power law (reviewed in Simoncelli and Olshausen 2001). Instead, the spectral frequency content of natural vestibular stimuli decreases relatively slowly over the low-frequency range (below ∼5 Hz) and more rapidly over higher frequencies (Carriot *et al*. 2014). In the present study, we observed this same pattern in patients with vestibular loss, where the corresponding 'transition frequencies' remained in the ∼5 Hz range (Fig. 1). Prior studies have shown that the unique stimulus structure of vestibular input experienced during voluntary behaviours is the result of active motion as well as passive biomechanical filtering (Carriot *et al*. 2014). Thus, this transformation appears to be a fundamental aspect of the statistical structure of vestibular stimuli, which is not altered following a vestibular loss.

Impaired updating of the internal models of voluntary movements *versus* reduced efficacy of postural reflexes

The main goal of our study was to investigate the role of vestibular feedback on the statistical structure of the head movements occurring during voluntary activities. To do this, we measured six-dimensional head movements in patients with vestibular hypofunction during active dynamic tasks that were designed to represent the full range of movements generated during everyday activities and included walking on foam, jumping and hopping, locomoting around obstacles and a self-motivated dish-sorting task. Such voluntary behaviours require precisely coordinated movements of multiple body parts and are characterized by 'repetition without repetition' (Bernstein, 1967). Thus, for example, there will be variability across steps in the 'walking on foam' task for each subject. Based on theoretical and behavioural studies, there are many reasons to believe that the brain ensures the accuracy of voluntary movements via a cerebellum-based mechanism that predicts the sensory consequences of motor commands (Miall & Wolpert, 1996; Lackner & DiZio, 2005; reviewed in Popa & Ebner,

2019). The difference between this internal prediction and the actual sensory consequences of movement is termed the sensory prediction error, and the prevailing view is that the cerebellum-based mechanism(s) require(s) online feedback to compute sensory prediction errors to ensure movement accuracy (Brooks *et al*. 2015; Mackrous *et al*. 2019).

In the present study, subjects had access to multiple sources of feedback, signalling the actual sensory consequences of movement (e.g. vestibular, visual, somatosensory). Accordingly, to ensure movement accuracy, the brain could compare this information with its internal prediction of the sensory consequences of voluntary behaviours. Notably, our patient group would have had less reliable vestibular feedback compared with our controls. The brain's reliance on different sources of sensory feedback is dependent on the relative noise of each (with less noisy estimates having greater weight, Ernst & Banks, 2002; van Beers 2009). As a consequence, patients with vestibular loss tend to upweight their reliance on other sensory cues (i.e. visual and proprioceptive feedback), particularly at higher frequencies where vestibular signals normally play the dominant role (Peterka & Loughlin, 2004; Peterka *et al*. 2011,2018). Additionally, behavioural studies in both humans and monkeys have shown that the upweighting of predictive motor signals further contribute to compensation (e.g. Dichgans *et al*. 1973, Della Santina *et al*. 2002, Sadeghi *et al*. 2010, 2012). This reweighting of sensory inputs and motor predictions occurs rapidly after unilateral vestibular loss and is mediated by the unmasking of these extravestibular cues at the first central stages of vestibular processing (Sadeghi *et al*. 2010, 2011, 2012; Jamali *et al*. 2014). Interestingly, such upweighting of extravestibular cues (e.g. sensory and motor predictions) in our patients was sufficient to ensure that normal head motion was indistinguishable in both the temporal and frequency domains during most of the tasks in the present study.

Importantly, however, patients demonstrated significantly greater head motion power at higher frequencies compared with controls during specific behaviours that likely required robust online feedback control. Specifically, patients generated greater head motion power during the 'jumping' task, which, in addition to being highly dynamic, was not a common behaviour for most subjects. Additionally, patients experienced greater head motion power during 'walking on foam' task, which is notable in that it was specifically designed to reduce the reliability of somatosensory feedback (Mulavara *et al*. 2009; Cohen *et al*. 2012). Thus, the upweighting of visual feedback, which is a relatively slow sensory system and thus is less effective at higher frequencies (reviewed in Desmurget & Grafton 2000), was unable to fully compensate for the loss of vestibular feedback during these tasks. We further speculate that the movement predictability was relatively lower during these more challenging tasks. Decreases in movement predictability have been linked to an increased reliance in vestibular sensory signals for estimating head movement (MacNeilage and Glasauer, 2017, Dietrich *et al*. 2020). Thus, it is likely that patients showed significant differences during these specific tasks, since their requirements for online sensory feedback to correct for unpredictable motion distinction were the most challenging.

Interestingly, for both tasks, our modelling results suggest that increased frequency-specific head-on-torso motion variability underlies the observed increase in head movement power (Fig. 6*C* & *D*). One possibility is that central changes in vestibulospinal pathways increase the variability in head-on-torso stabilization responses of unilateral vestibular patients. Previous behavioural (Igarashi & Guitierrez, 1983), electromyography (Lacour *et al*. 1979; Lindsay & Rosenberg, 1977; Dutia *et al*. 1985), and electrophysiology (Sadeghi *et al*. 2011) experiments have shown that the efficacy of vestibulospinal reflexes recovers to normal values within 2–3 weeks following unilateral vestibular loss. It is noteworthy that the studies above measured averaged gain and phase but not variability. Importantly, however, neurons at the first stage of central processing (i.e. vestibular nuclei) show an increase in trial-to-trial neuronal variability following unilateral vestibular loss that persists over time (Jamali *et al*. 2014). This increased variability could then, in turn, lead to increased variability of vestibulospinal pathways that generate compensatory head–torso movements (Peng *et al*. 1996, Goldberg & Cullen, 2011). Here we have focused on head–torso coupling; future studies using an additional cervical sensor would further enable analysis of the contributions of head–neck coupling.

Current evidence suggests that the accurate calibration and control of voluntary self-motion requires the central nervous system to generate an internal model of the predicted sensory consequences of head motion that it dynamically compares with the actual sensory feedback (reviewed in Cullen 2019). Notably, internal models appear to employ probabilistic models to learn the distribution (i.e. average and variability) of the sensory feedback (Körding & Wolpert 2004; Ma & Jazayeri 2014). Thus, while noisy vestibular feedback would not affect the average predictions, it is also possible that the increased noise in the vestibular feedback (i.e. the observed increase in head–torso gain/phase variability) adds uncertainly to the predictions of the brain's internal models. In this context, compromised feedback to internal models could have also contributed to the marked changes observed in patient head motion statistics during challenging voluntary tasks that require rapid online feedback control (i.e. 'walking on foam' and 'jumping').

References

Armand M & Minor LB (2001). Relationship between time- and frequency-domain analyses of angular head movements in the squirrel monkey. *J Comput Neurosci* **11**, 217–239.

Baloh RW, Honrubia V & Kerber KA (2010). *Baloh and Honrubia's clinical neurophysiology of the vestibular system*. Contemporary Neurology. **77** 4, Oxford University Press, 149–169.

Bernstein NA (1967). *The Co-ordination and Regulation of Movements*. Pergamon Press.

Brooks JX, Carriot J & Cullen KE (2015). Learning to expect the unexpected: rapid updating in primate cerebellum during voluntary self-motion. *Nat Neurosci* **18**, 1310–1317.

Carriot J, Jamali M, Chacron MJ & Cullen KE (2014). Statistics of the vestibular input experienced during natural self-motion: implications for neural processing. *J Neurosci* **34**, 8347–8357.

Carriot J, Jamali M, Cullen KE & Chacron MJ (2017*a*). Envelope statistics of self-motion signals experienced by human subjects during everyday activities: Implications for vestibular processing. *PLoS One* **12**, e0178664.

Carriot J, Jamali M, Chacron MJ & Cullen KE (2017*b*). The statistics of the vestibular input experienced during natural self-motion differ between rodents and primates. *J Physiol* **595**, 2751–2766.

Clark TK, Newman MC, Karmali F, Oman CM & Merfeld DM (2019). Mathematical models for dynamic, multisensory spatial orientation perception. *Prog Brain Res* **248**, 65–90.

Cohen HS, Mulavara AP, Peters BT, Sangi-Haghpeykar H & Bloomberg JJ (2012). Tests of walking balance for screening vestibular disorders. *J Vestib Res* **22**, 95–104.

Cullen KE (2019). Vestibular processing during natural self-motion: implications for perception and action. *Nat Rev Neurosci* **20**, 346–363.

Della Santina CC, Cremer PD, Carey JP & Minor LB (2002). Comparison of head thrust test with head autorotation test reveals that the vestibulo-ocular reflex is enhanced during voluntary head movements. *Arch Otolaryngol Head Neck Surg* **128**, 1044–1054.

Desmurget M & Grafton S (2000). Forward modeling allows feedback control for fast reaching movements. *Trends Cogn Sci* **4**, 423–431.

Dichgans J, Bizzi E, Morasso P & Tagliasco V (1973). Mechanisms underlying recovery of eye-head coordination following bilateral labyrinthectomy in monkeys. *Exp Brain Res* **18**, 548–562.

Dietrich H, Heidger F, Schniepp R, MacNeilage PR, Glasauer S & Wuehr M (2020). Head motion predictability explains activity-dependent suppression of vestibular balance control. *Sci Rep* **10**, 1–10.

Dutia MB (1985). Vestibular control of neck muscles in acute and chronic hemilabyrinthectomized cats. *J Physiol* **366**, 281–290.

Ernst MO & Banks MS (2002). Humans integrate visual and haptic information in a statistically optimal fashion. *Nature* **415**, 429–433.

Ferraris F, Grimaldi U & Parvis M (1995). Procedure for effortless in-field calibration of three-axis rate gyros and accelerometers. *Sens Mater* **7**, 311–330.

Goldberg JM & Cullen KE (2011). Vestibular control of the head: possible functions of the vestibulocollic reflex. *Exp Brain Res* **210**, 331-345

Goldberg JM, Wilson VJ, Angelaki DE, Cullen KE, Broussard, DM, Fukushima, K, Buttner-Ennever, J & Minor, LB (2012). *The Vestibular System: A Sixth Sense*. USA: Oxford University Press.

Hausamann P, Daumer M, MacNeilage PR & Glasauer S (2019). Ecological momentary assessment of head motion: toward normative data of head stabilization. *Front Hum Neurosci* **13**, 179.

Hullar TE, Zee DS & Minor LB (2010). Evaluation of the patient with dizziness. In *Cummings Otolaryngology - Head and Neck Surgery*, Paul W. Flint & Charles William Cummings, Mosby/Elsevier, pp. 2305–2327.

Huterer M & Cullen KE (2002). Vestibuloocular reflex dynamics during high-frequency and high-acceleration rotations of the head on body in rhesus monkey. *J Neurophysiol* **88**, 13–28.

Igarashi M & Guitierrez O (1983). Analysis of righting reflex in cats with unilateral and bilateral labyrinthectomy. *ORL* **45**, 279–289.

Jamali M, Mitchell DE, Dale A, Carriot J, Sadeghi SG & Cullen KE (2014). Neuronal detection thresholds during vestibular compensation: contributions of response variability and sensory substitution. *J Physiol* **592**, 1565-1580.

Körding KP & Wolpert DM (2004). Bayesian integration in sensorimotor learning. *Nature* **427**, 244–247.

Lackner JR & DiZio P (2005). Motor control and learning in altered dynamic environments. *Curr Opin Neurobiol* **15**, 653–659.

Lacour M, Xerri C & Hugon M (1979). Compensation of postural reactions to fall in the vestibular neurectomized monkey. Role of the remaining labyrinthine afferences. *Exp Brain Res* **37**, 563–580.

Lindsay KW & Rosenberg JR (1977). The effect of cerebellectomy on tonic labyrinth reflexes in the forelimb of the decerebrate cat. *J Physiol* **273**, 76–77.

Ma WJ & Jazayeri M (2014). Neural coding of uncertainty and probability. *Annu Rev Neurosci* **37**, 205–220.

Mackrous I, Carriot J, Jamali M & Cullen KE (2019). Cerebellar prediction of the dynamic sensory consequences of gravity. *Curr Biol* **29**, 2698-2710.e4.

MacNeilage PR & Glasauer S (2017). Quantification of head movement predictability and implications for suppression of vestibular input during locomotion. *Front Comput Neurosci* **11**, 47.

Macpherson JM & Fung J (1999). Weight support and balance during perturbed stance in the chronic spinal cat. *J Neurophysiol* **82**, 3066–3081.

Massot C, Schneider AD, Chacron MJ & Cullen KE (2012). The vestibular system implements a linear–nonlinear transformation in order to encode self-motion. *PLoS Biol* **10**, e1001365.

Mergner T, Siebold C, Schweigart G & Becker W (1991). Human perception of horizontal trunk and head rotation in space during vestibular and neck stimulation. *Exp Brain Res* **85**, 389–404.
Miall RC & Wolpert DM (1996). Forward Models for Physiological Motor Control. *Neural Networks* **9**, 1265–1279.
Mijovic T, Carriot J, Zeitouni A & Cullen KE (2014). Head movements in patients with vestibular lesion: a novel approach to functional assessment in daily life setting. *Otol Neurotol* **35**, e348.
Minor LB (1998). Gentamicin-induced bilateral vestibular hypofunction. *JAMA* **279**, 541–544.
Miyamoto YR, Wang S & Smith MA (2020). Implicit adaptation compensates for erratic explicit strategy in human motor learning. *Nat Neurosci* **23**, 443–455.
Mulavara AP, Cohen HS & Bloomberg JJ (2009). Critical features of training that facilitate adaptive generalization of over ground locomotion. *Gait Posture* **29**, 242–248.
Nnodim JO & Yung RL (2015). Balance and its clinical assessment in older adults–A review. *J Geriatr Med Gerontol* **1**, 003.
Paul SS, Dibble LE, Walther RG, Shelton C, Gurgel RK & Lester ME (2017). Characterization of head-trunk coordination deficits after unilateral vestibular hypofunction using wearable sensors. *JAMA Otolaryngol Head Neck Surg* **143**, 1008–1014.
Paul SS, Dibble LE, Walther RG, Shelton C, Gurgel RK & Lester ME (2018). Reduced purposeful head movements during community ambulation following unilateral vestibular loss. *Neurorehabil Neural Repair* **32**, 309-316.
Peng GC, Hain TC & Peterson BW (1996). A dynamical model for reflex activated head movements in the horizontal plane. *Biol Cybern* **75**, 309–319.
Peterka RJ & Loughlin PJ (2004). Dynamic regulation of sensorimotor integration in human postural control. *J Neurophysiol* **91**, 410–423.
Peterka RJ, Statler K, Wrisley D & Horak F (2011). Postural compensation for unilateral vestibular loss. *Front Neurol* **2**, 57.
Peterka RJ. Sensory integration for human balance control (2018). *Handb Clin Neurol* **159**, 27–42.
Popa LS & Ebner TJ (2019). Cerebellum, Predictions and Errors. *Front Cell Neurosci* **12**, 524.
Pozzo T, Berthoz A, Vitte E & Lefort L (1991). Head Stabilization during Locomotion: Perturbations Induced by Vestibular Disorders. *Acta Oto-laryngol* **111**, 322–327.
Sadeghi SG, Minor LB & Cullen KE (2010). Neural correlates of motor learning in the vestibulo-ocular reflex: dynamic regulation of multimodal integration in the macaque vestibular system. *J Neurosci* **30**, 10158–10168.
Sadeghi SG, Minor LB & Cullen KE (2011). Multimodal integration after unilateral labyrinthine lesion: single vestibular nuclei neuron responses and implications for postural compensation. *J Neurophysiol* **105**, 661–673.
Sadeghi SG, Minor LB & Cullen KE (2012). Neural correlates of sensory substitution in vestibular pathways following complete vestibular loss. *J Neurosci* **32**, 14685–14695.
Sağlam M, Glasauer S & Lehnen N (2014). Vestibular and cerebellar contribution to gaze optimality. *Brain* **137**, 1080–1094.
Simoncelli EP & Olshausen BA (2001). Natural Image Statistics and Neural Representation. *Annu Rev Neurosci* **24**, 1193–1216.
Strupp M & Magnusson M (2015). Acute unilateral vestibulopathy. *Neurol Clin* **33**, 669–685.
van Beers RJ (2009). Motor learning is optimally tuned to the properties of motor noise. *Neuron* **63**, 406–417.
Wrisley DM, Marchetti GF, Kuharsky DK & Whitney SL (2004). Reliability, Internal Consistency, and Validity of Data Obtained With the Functional Gait Assessment. *Phys Ther* **84**, 906–918.
Zobeiri OA, Mischler GM, King SA, Lewis RF & Cullen KE (2021). Effects of vestibular neurectomy and neural compensation on head movements in patients undergoing vestibular schwannoma resection. *Sci Rep* **11**, 517.

Additional information

Data availability statement

The data that support the findings of this study have been deposited on Figshare under the URL. https://doi.org/10.6084/m9.figshare.13656404.

Competing interests

The authors declare that they have no conflicts of interest.

Author contributions

O.A.Z., K.E.C. and Y.A. designed the study. B.O. and Y.A. performed the experiments. O.A.Z. analysed the data. O.A.Z. prepared figures and tables. K.E.C. and O.A.Z. wrote the paper with input from Y.A.

Funding

This work was funded by grants R01-DC002390, R01-DC018061 and 1UF1NS111695-01) from the National Institutes of Health (KEC).

Acknowledgements

We thank Robyn Mildren, Pum Wiboonsaksakul and Oliver Stanley for their helpful feedback on the manuscript. We also thank Jerome Carriot for his comments and for his assistance with the conceptualization of figures schematics.

Keywords

balance, natural statistics, self-motion, vestibular system

Supporting information

Additional supporting information may be found online in the Supporting Information section at the end of the article.

Statistical Summary Document